Am J Transl Res 2026;18(7):5941-5953
www.ajtr.org /ISSN:1943-8141/AJTR0172992

Original Article

Imaging signatures of distinct crystal deposition on high-frequency ultrasound for differentiating gouty arthritis and calcific tendinitis

Yun Lin[1*], Guangling Li[1*], Xinna Li[1*], Jinli Kou[2], Lan Zhang[3], Ying Zhang[2], Hui Feng[4], Chang Lu[5], Juanchou Ji[6], Wei Wang[1#], Hongyan Zhao[7#], Hehuan Zhang[4#]

[1]Department of Medical Technology Support, Jingzhong Medical Area, PLA General Hospital, Beijing 100120, China; [2]Department of General Surgery, Jingzhong Medical Area, PLA General Hospital, Beijing 100120, China; [3]Department of Outpatient, Jingzhong Medical Area, PLA General Hospital, Beijing 100120, China; [4]Department of Zhantansi Outpatient, Jingzhong Medical Area, PLA General Hospital, Beijing 100034, China; [5]Department of Fuxinglu Outpatient, Jingnan Medical Area, PLA General Hospital, Beijing 100161, China; [6]Department of General Internal Medicine, Jingzhong Medical Area, PLA General Hospital, Beijing 100120, China; [7]Department of Lishilu Outpatient, Jingzhong Medical Area, PLA General Hospital, Beijing 100842, China. [*]Equal contributors and co-first authors. [#]co-corresponding authors.

Received March 30, 2026; Accepted May 18, 2026; Epub July 15, 2026; Published July 30, 2026

Abstract: Aims: To compare high-frequency ultrasound imaging signatures of crystal deposition in gouty arthritis (GA) and calcific tendinitis (CT), and explore their value in non-invasive differential diagnosis. Methods: This single-center retrospective study enrolled 130 subjects from, including 50 GA patients, 40 CT patients and 40 healthy controls. All received standardized high-frequency ultrasound to observe lesion distribution, deposit morphology, quantitative sonographic metrics, inflammatory findings, and dynamic imaging features. We compared ultrasonic characteristics between groups, and adopted ROC curves and multivariate logistic regression to evaluate the differential diagnostic efficiency of ultrasound indicators. Results: Crystal depositions were commonly detected in GA and CT patients but rarely in healthy controls. GA tended to present bilateral and multifocal lesions mainly distributed in synovium and cartilage of foot, ankle and knee joints with numerous small, shallow and irregular deposits, accompanied by obvious intra-articular inflammation. CT predominantly affected shoulder tendons, manifested as large, deep, homogeneous and highly echogenic deposits with marked posterior acoustic shadowing, together with more peritendinous inflammatory changes. Shoulder-predominant involvement yielded the highest differential diagnostic efficacy with an AUC of 0.932. Conclusion: High-frequency ultrasound can effectively distinguish GA from CT based on distinctive lesion distribution, crystal morphology and accompanying inflammatory manifestations, serving as a reliable non-invasive differential diagnostic tool.

Keywords: High-frequency ultrasound, crystal deposition, gouty arthritis, calcific tendinitis, differential diagnosis

Introduction

Crystal-induced musculoskeletal disease is a significant type of painful and debilitating disease encountered in rheumatology, sports medicine, and musculoskeletal imaging [1]. Two common forms are gouty arthritis (GA) and calcific tendinitis (CT), both of which are pathologically characterized by crystal deposition, but they differ substantially in biochemical composition, anatomic predilection, inflammatory response, clinical course, and treatment strategy. Deposition of monosodium urate crystals, which are usually found in synovial structures, articular cartilage, tendon sheaths [2], and periarticular soft tissues, causes gout; whereas, CT is largely related to deposition of calcium hydroxyapatite in tendons, most commonly in the rotator cuff [3]. In GA, crystal deposition tends to involve articular and periarticular structures and is often associated with recurrent acute inflammatory attacks, synovitis, joint effusion, and, in chronic cases, tophus formation and bone erosion. By contrast, CT is primarily a localized tendon disorder, usually characterized by focal intratendinous calcific

https://doi.org/10.62347/TOAS3612

deposits, tendon thickening, peri-tendinous edema, bursitis, and pain related to mechanical impingement or the resorptive phase of calcification. Thus, although both conditions are crystal-related disorders, GA is more closely linked to systemic metabolic disturbance and joint-based inflammation, whereas CT is more often associated with localized tendon pathology and peri-tendinous tissue reaction. Despite these essential distinctions, the acute clinical presentations, such as pain, swelling, tenderness, and limited motion can overlap, creating diagnostic uncertainty, especially in atypical manifestations or when joint aspiration is impractical.

Clinically, it is necessary to properly distinguish between GA and CT, as their treatment plans, long-term follow-up, and prognostic implications differ. Urate-lowering therapy and management of systemic metabolic risk factors [4, 5] are often used to manage gout, whereas conventional conservative therapy, image-guided procedures, or, in rare cases, surgery are used to treat CT [6-9]. In addition, the two entities may show different imaging patterns because of their distinct crystal-tissue interactions: gout more often produces surface-related, multifocal, and irregular deposits involving cartilage and synovial structures, whereas CT usually presents as localized, dense, intratendinous calcification, often with marked posterior acoustic shadowing. Traditional diagnostic methods rely on clinical history, laboratory testing, radiography, dual-energy computed tomography, or microscopic crystal confirmation, but all have limitations in sensitivity, accessibility, invasiveness, or dynamic soft-tissue evaluation capacity. In practice, a rapid, noninvasive, and widely accessible imaging modality that depicts crystal deposition patterns with sufficient accuracy to aid differential diagnosis is still required.

High-frequency ultrasound (HFUS) has become useful in imaging superficial joints, tendons, and periarticular soft tissues due to its high spatial resolution, real-time capability, lack of ionizing radiation, and ability to reveal both morphologic abnormalities and inflammatory conditions [10, 11]. Ultrasound has been found to detect a range of typical appearances in gout, such as the double contour sign, tophi, erosions, and synovial hypertrophy [12]. In CT, it can delineate intratendinous calcific foci, posterior acoustic behavior, and associated bursitis or hyperemia [13]. Nevertheless, most previous studies have described disease-specific sonographic features in isolation rather than systematically comparing the imaging characteristics of different crystal deposits in these two conditions. Consequently, the differential diagnostic value of ultrasound based on crystal morphology, distribution, echogenic pattern, and tissue response remains inadequately defined.

Pathobiologically, the imaging manifestations of GA and CT should not be viewed as merely descriptive but rather as indicative of fundamentally different crystal-tissue interactions. Monosodium urate crystals tend to deposit on cartilage surfaces and synovial-lined structures, frequently producing hyperechoic linear deposits with inflammatory synovitis, whereas hydroxyapatite crystals are more likely to deposit within the tendon substance and show variable echotexture depending on the stage of calcific evolution and resorption [14]. These deposition patterns can be systematically characterized by ultrasound, and such systematic characterization may provide diagnostically meaningful imaging signatures that discriminate between diseases more effectively than symptom analysis alone.

The present study aimed to investigate the HFUS features of distinct crystal deposition in GA and CT and to identify imaging markers with differential diagnostic value. By comparing the location, morphology, echogenic characteristics, distribution pattern, and associated soft-tissue changes of crystal deposits in these two conditions, we sought to establish an imaging framework for more accurate, noninvasive differentiation. Such an approach may not only enhance diagnostic confidence in daily clinical practice but also deepen understanding of the sonographic expression of crystal-related musculoskeletal disease.

Methods

Study design

This retrospective observational study was conducted in a single center to explore the HFUS characteristics of distinct crystal deposition patterns in GA and CT and to determine their diagnostic utility in differential diagnosis.

Consecutive participants evaluated at Jingzhong Medical Area, PLA General Hospital between September 2021 and December 2025 were identified from the electronic medical record and imaging database. The sample of 130 individuals was divided into three groups: GA (Group 1, n = 50), CT (Group 2, n = 40), and healthy controls (Group 3, n = 40). For the GA group, eligible participants were adults aged 18 years or older who met the diagnostic criteria for GA based on a combination of clinical presentation, laboratory findings, and confirmatory imaging and/or crystal evidence when available. Specifically, the diagnosis was established in patients with typical episodes of acute or recurrent inflammatory arthritis together with at least one of the following: (1) identification of monosodium urate crystals in synovial fluid or tophus aspirate; (2) hyperuricemia in the appropriate clinical setting; or (3) imaging findings supportive of gout, as documented in the medical record by the treating clinician. Only patients with a definite final clinical diagnosis of GA, adequate high-frequency ultrasound images, and complete clinical records were included.

For the CT group, eligible participants were adults aged 18 years or older with a definite diagnosis of CT based on compatible clinical symptoms and imaging evidence of calcific deposition within the tendon. The diagnosis required the presence of localized tendon-related pain and/or functional limitation corresponding to the affected site, together with imaging confirmation of intratendinous calcific deposits on ultrasound and/or other conventional imaging modalities as recorded in the medical chart. Patients were included only when the final diagnosis of CT had been clearly documented and sufficient ultrasound images and clinical data were available for review.

Healthy controls were individuals without a history of gout, crystal arthropathy, inflammatory arthritis, tendon calcification, autoimmune disease, or chronic musculoskeletal symptoms, and without abnormal ultrasound findings suggestive of crystal deposition or active musculoskeletal pathology.

Exclusion criteria for all groups were as follows: incomplete clinical or imaging data; ultrasound images of insufficient quality for reliable interpretation; previous surgery, invasive intervention, or major trauma involving the examined joint or tendon; and comorbid conditions that could substantially confound sonographic assessment, including infectious arthritis, malignancy, severe osteoarthritis, or other rheumatic diseases. Individuals with uncertain diagnoses, non-crystal-related musculoskeletal disorders, or repeated examinations during the study period were also excluded; in such cases, only the first eligible examination was included (**Figure 1**). Clinical records, laboratory results, and ultrasound images were reviewed according to a standardized protocol. The study was approved by the institutional ethics committee of Jingzhong Medical Area, PLA General Hospital and conducted in accordance with the Declaration of Helsinki.

Data collection and outcome measures

At study entry, we gathered demographic and clinical information, including age, sex, body mass index, smoking and alcohol use, and key comorbidities such as hypertension, hyperlipidemia, diabetes mellitus, cardiovascular disease, and chronic kidney disease. Participants then underwent a standardized HFUS examination performed according to a predefined protocol. This examination systematically assessed lesion presence, anatomical distribution, and imaging burden across articular, periarticular, and tendon-related sites. Quantitative sonographic measurements were obtained for each detectable deposit, including maximum length, breadth, approximate area, thickness, depth from the skin surface, number of individual deposits, echogenicity-related measures, posterior acoustic shadowing, margin irregularity, and surface coverage area. Additionally, we documented relevant inflammatory and structural abnormalities, such as joint effusion, synovial hypertrophy, synovitis grade, Power Doppler activity, tendon thickening, peritendinous edema, bursitis, cortical irregularity, and bone erosion. Dynamic ultrasound changes and perilesional responses were also evaluated, including pain provocation, gliding restriction, mechanical impingement, bursal friction, deposit displacement, reactive hyperemia, synovial proliferation, and secondary tissue changes.

From these evaluations, we derived a comprehensive set of prespecified composite imaging indicators that enabled nuanced differentiation

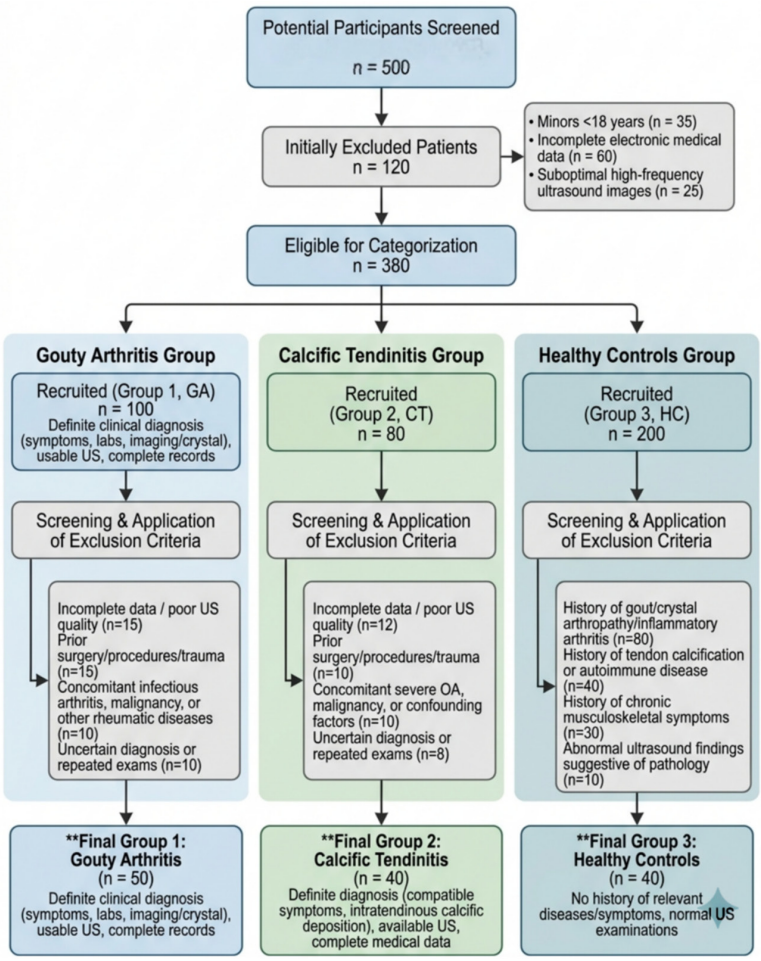

Figure 1. Participant enrollment and group assignment flowchart.

between GA and CT. These indicators included the double-contour sign, synovial involvement, cartilage surface deposition, intratendinous deposits, heterogeneous aggregate patterns, posterior acoustic shadowing, arc-shaped calcification, and shoulder-dominant involvement. Each of these features was systematically evaluated both in isolation and in combination to characterize their distinct contributions to the diagnostic process. For instance, the double-contour sign, predominantly observed in GA, was indicative of monosodium urate crystal deposition along articular cartilage. Synovial involvement and cartilage surface deposition were also key markers for GA, reflecting active inflammation and crystal deposition within synovial and cartilaginous structures. In contrast, CT was characterized by intratendinous deposits, arc-shaped calcification, and posterior acoustic shadowing, all associated with hydroxyapatite crystal deposition. Furthermore, dynamic features such as shoulder-dominant involvement played a critical role in distinguishing CT, which predominantly affects the shoulder tendons. These composite imaging indicators were then analyzed using receiver operating characteristic curves and multivariate logistic regression to assess their individual and collective ability to distinguish between GA and CT. This analysis enabled us to identify the most effective imaging markers for noninvasive differentiation of these two conditions.

Statistical analysis

Statistical tests were conducted to compare demographic and patient characteristics as well as HFUS features among the GA, CT, and healthy control groups, and to determine the imaging features that distinguished between GA and CT. For continuous variables, depending on their distribution, data were summarized as mean ± standard deviation or median (interquartile range). Categorical variables were presented as counts and percentages. One-way analysis of variance or the Kruskal-Wallis test was used for between-group comparisons of continuous variables as appropriate, while the chi-square test or Fisher's exact test was used for categorical variables. To establish the primary diagnostic comparison between GA and CT, candidate HFUS variables were preselected based on clinical relevance and univariate discriminatory performance, including lesion topography, morphologic deposition patterns, inflammatory findings, and the presence of secondary structural alterations. The diagnostic performance of individual imaging characteristics was quantified using receiver operating characteristic (ROC) curve analysis, from which the area under the curve (AUC) and respective 95% confidence intervals (CIs) were calculated.

Table 1. Demographic and clinical characteristics

Variable	Group 1: Gouty arthritis (n = 50)	Group 2: Calcific tendinitis (n = 40)	Group 3: Healthy controls (n = 40)	χ^2/t	*P* value
Age, years	53.36 ± 11.63	56.08 ± 10.90	47.08 ± 11.17	F = 6.762	0.002
Male sex, n (%)	41 (82.0)	14 (35.0)	22 (55.0)	χ^2 = 20.757	<0.001
Body mass index, kg/m^2	29.19 ± 4.05	25.03 ± 3.94	23.45 ± 3.33	F = 27.637	<0.001
Current smoking, n (%)	14 (28.0)	8 (20.0)	7 (17.5)	χ^2 = 1.591	0.451
Current alcohol use, n (%)	24 (48.0)	10 (25.0)	9 (22.5)	χ^2 = 8.231	0.016
Hypertension, n (%)	27 (54.0)	13 (32.5)	8 (20.0)	χ^2 = 11.515	0.003
Diabetes mellitus, n (%)	11 (22.0)	5 (12.5)	2 (5.0)	χ^2 = 5.471	0.065
Hyperlipidemia, n (%)	23 (46.0)	11 (27.5)	6 (15.0)	χ^2 = 10.315	0.006
Chronic kidney disease, n (%)	9 (18.0)	2 (5.0)	1 (2.5)	χ^2 = 7.606	0.022
History of cardiovascular disease, n (%)	7 (14.0)	4 (10.0)	2 (5.0)	χ^2 = 2.000	0.368

Multivariate logistic regression analysis was conducted to identify independent imaging variables associated with disease classification, with diagnosis (GA vs. CT) as the dependent variable; adjusted odds ratios (ORs) with 95% confidence intervals were reported. Variables with high biological plausibility and discriminatory ability were entered into the multivariate model, with consideration of collinearity and overfitting. All statistical tests were two-sided, and a *P* value below 0.05 was considered statistically significant.

Results

Demographic and clinical characteristics

Significant between-group differences were observed for age, sex distribution, body mass index, alcohol use, hypertension, hyperlipidemia, and chronic kidney disease (all P<0.05). Overall, patients with GA showed a predominantly male and more metabolically unfavorable profile, whereas patients with CT were older and had a more balanced sex distribution. By contrast, healthy controls exhibited the most favorable baseline characteristics across most variables. No significant between-group differences were found for current smoking, history of cardiovascular disease, or diabetes mellitus, although the latter showed a nonsignificant trend toward higher prevalence in the GA group (P = 0.065) (**Table 1**). These findings indicate that the three groups were broadly distinguishable in their baseline demographic and comorbidity patterns, particularly with respect to sex and metabolic burden.

Anatomic distribution and lesion burden on HFUS

Detectable focal deposits were identified in nearly all patients with GA and CT (94.0% [47/50] and 95.0% [38/40], respectively), whereas no deposits were observed in healthy controls (0/40; P<0.001). Compared with CT, GA showed a significantly greater disease burden, with more frequent bilateral involvement (38.0% vs. 17.5%; P<0.001) and a higher proportion of multifocal lesions involving at least two sites (58.0% vs. 27.5%; P<0.001). The distribution pattern also differed markedly between the two disease groups. In GA, deposits predominantly involved synovial structures (70.0%), cartilage surfaces (52.0%), and lower-extremity sites, particularly the foot/ankle (62.0%) and knee (34.0%), all with significant differences across groups (all P<0.001). By contrast, CT was characterized by a strong predilection for tendon involvement (95.0%) and the shoulder (92.5%), with only limited synovial (5.0%) or cartilage surface involvement (2.5%) (**Table 2**).

Quantitative ultrasound metrics of deposits

Compared with GA, CT exhibited significantly larger deposits, with greater maximum deposit length (1.71 ± 0.27 vs. 1.40 ± 0.20 mm), maximum deposit width (1.49 ± 0.24 vs. 1.44 ± 0.20 mm), calculated deposit area (11.50 ± 1.82 vs. 8.87 ± 1.26 mm^2), and deposit thickness (1.29 ± 0.20 vs. 0.56 ± 0.08 mm; all P<0.001). By contrast, GA was characterized by a greater number of discrete deposits within

Table 2. Anatomic distribution and lesion burden on high-frequency ultrasound

Variable	Group 1: Gouty arthritis (n = 50)	Group 2: Calcific tendinitis (n = 40)	Group 3: Healthy controls (n = 40)	χ^2/t	*P* value
Patients with detectable focal deposits, n (%)	47 (94.0)	38 (95.0)	0 (0)	χ^2 = 109.146	<0.001
Bilateral involvement, n (%)	19 (38.0)	7 (17.5)	0 (0)	χ^2 = 20.281	<0.001
Multifocal lesions (≥2 sites), n (%)	29 (58.0)	11 (27.5)	0 (0)	χ^2 = 35.383	<0.001
Synovial involvement, n (%)	35 (70.0)	2 (5.0)	0 (0)	χ^2 = 69.099	<0.001
Tendon involvement, n (%)	21 (42.0)	38 (95.0)	1 (2.5)	χ^2 = 69.422	<0.001
Cartilage surface involvement, n (%)	26 (52.0)	1 (2.5)	0 (0)	χ^2 = 48.235	<0.001
Foot/ankle involvement, n (%)	31 (62.0)	0 (0)	0 (0)	χ^2 = 65.131	<0.001
Knee involvement, n (%)	17 (34.0)	3 (7.5)	0 (0)	χ^2 = 22.493	<0.001
Shoulder involvement, n (%)	3 (6.0)	37 (92.5)	1 (2.5)	χ^2 = 99.572	<0.001

each lesion field (1.13 ± 0.16 vs. 0.77 ± 0.12; P<0.001), consistent with a more fragmented and multifocal deposition pattern. Lesions in CT were located deeper from the skin surface than those in GA (2.43 ± 0.38 vs. 1.10 ± 0.16 mm; P<0.001). Both groups demonstrated an echogenicity ratio relative to adjacent soft tissue of 0.12 ± 0.02, but CT showed lower gray-scale intensity (19.60 ± 3.10 vs. 23.54 ± 3.33 arbitrary units) and more pronounced posterior acoustic shadowing (0.11 ± 0.02 vs. 0.09 ± 0.01; all P<0.001). In contrast, gouty deposits displayed significantly greater margin irregularity (0.57 ± 0.08 vs. 0.31 ± 0.05; P<0.001) and lower surface coverage along cartilage/tendon interfaces (9.78% ± 1.38% vs. 12.72% ± 2.01%; P<0.001). Although both disease groups had markedly higher total sonographic burden scores than healthy controls (1.74 ± 0.25 for GA and 1.66 ± 0.26 for CT vs. 0.02 ± 0.002; P<0.001), the composite quantitative profile suggests that GA is typified by multiple smaller, shallower, irregular deposits, whereas CT is characterized by fewer but larger, deeper deposits with more pronounced posterior acoustic shadowing (**Table 3**).

Inflammatory activity and associated soft-tissue abnormalities

GA showed substantially greater intra-articular inflammatory activity, with higher frequencies of joint effusion (56.0% vs. 15.0% vs. 2.5%), synovial hypertrophy (50.0% vs. 10.0% vs. 0%), and moderate-to-severe synovitis (synovitis grade ≥2:36.0% vs. 5.0% vs. 0%), all significantly different across groups (all P<0.001). Power Doppler findings further supported more active synovial vascular inflammation in GA, with a higher prevalence of Doppler positivity (42.0% vs. 25.0% vs. 0%; P<0.001). In contrast, CT was characterized predominantly by peri-tendinous and bursal abnormalities, including more frequent tendon thickening (75.0% vs. 22.0% vs. 5.0%), peritendinous edema (57.5% vs. 16.0% vs. 0%), bursal distention (40.0% vs. 18.0% vs. 0%), subacromial-subdeltoid bursitis (37.5% vs. 0% vs. 0%), and soft-tissue edema adjacent to the deposit (60.0% vs. 34.0% vs. 0%), with all between-group differences reaching statistical significance (all P<0.001). Structural damage patterns also differed: bone erosion was significantly more common in GA than in CT and healthy controls (30.0% vs. 5.0% vs. 0%; P<0.001), whereas cortical irregularity without definite erosion did not differ significantly between groups (26.0% vs. 20.0% vs. 25.0%; P = 0.785) (**Table 4**).

Dynamic ultrasound findings

Dynamic scanning more often provoked pain (44.0% vs. 25.0%; P = 0.003), demonstrated mechanical impingement signs (96.0% vs. 35.0%; P<0.001), restricted gliding (90.0% vs. 40.0%; P<0.001), compression-induced synovial pain (42.0% vs. 12.5%; P = 0.002), motion-related bursal friction (98.0% vs. 62.5%; P<0.001), and reduced joint/tendon excursion (64.0% vs. 47.5%), although the latter did not reach statistical significance (P = 0.116). By contrast, CT was more frequently characterized by dynamic displacement of the deposit during movement or probe manipulation (32.5% vs.

Table 3. Quantitative ultrasound metrics of deposits

Variable	Group 1: Gouty arthritis (n = 50)	Group 2: Calcific tendinitis (n = 40)	Group 3: Healthy controls (n = 40)	F	*P* value
Maximum deposit length, mm	1.40 ± 0.20	1.71 ± 0.27	0	926.48	<0.001
Maximum deposit width, mm	1.44 ± 0.20	1.49 ± 0.24	0	268.622	<0.001
Calculated deposit area, mm^2	8.87 ± 1.26	11.50 ± 1.82	0	316.294	<0.001
Deposit thickness, mm	0.56 ± 0.08	1.29 ± 0.20	0	339.869	<0.001
Number of discrete deposits per lesion field	1.13 ± 0.16	0.77 ± 0.12	0	163.012	<0.001
Lesion depth from skin, mm	1.10 ± 0.16	2.43 ± 0.38	12.65 ± 2.00	531.084	<0.001
Echogenicity ratio to adjacent soft tissue	0.12 ± 0.02	0.12 ± 0.02	0	221.657	<0.001
Gray-scale intensity, arbitrary units	23.54 ± 3.33	19.60 ± 3.10	0.01 ± 0.001	336.396	<0.001
Margin irregularity score (0-3)	0.57 ± 0.08	0.31 ± 0.05	0.01 ± 0.002	281.648	<0.001
Acoustic shadow grade (0-3)	0.09 ± 0.01	0.11 ± 0.02	0	157.443	<0.001
Surface coverage along cartilage/tendon, %	9.78 ± 1.38	12.72 ± 2.01	0	127.754	<0.001
Total sonographic burden score (0-20)	1.74 ± 0.25	1.66 ± 0.26	0.02 ± 0.002	180.956	<0.001

Table 4. Inflammatory activity and associated soft-tissue abnormalities

Variable	Group 1: Gouty arthritis (n = 50)	Group 2: Calcific tendinitis (n = 40)	Group 3: Healthy controls (n = 40)	χ^2	*P* value
Joint effusion, n (%)	28 (56.0)	6 (15.0)	1 (2.5)	χ^2 = 36.504	<0.001
Synovial hypertrophy, n (%)	25 (50.0)	4 (10.0)	0 (0)	χ^2 = 37.105	<0.001
Synovitis grade ≥2, n (%)	18 (36.0)	2 (5.0)	0 (0)	χ^2 = 26.910	<0.001
Power Doppler positivity, n (%)	21 (42.0)	10 (25.0)	0 (0)	χ^2 = 21.629	<0.001
Tendon thickening, n (%)	11 (22.0)	30 (75.0)	2 (5.0)	χ^2 = 48.775	<0.001
Peritendinous edema, n (%)	8 (16.0)	23 (57.5)	0 (0)	χ^2 = 39.167	<0.001
Bursal distention, n (%)	9 (18.0)	16 (40.0)	0 (0)	χ^2 = 20.681	<0.001
Subacromial-subdeltoid bursitis, n (%)	0 (0)	15 (37.5)	0 (0)	χ^2 = 38.152	<0.001
Soft tissue edema adjacent to deposit, n (%)	17 (34.0)	24 (60.0)	0 (0)	χ^2 = 33.574	<0.001
Bone erosion, n (%)	15 (30.0)	2 (5.0)	0 (0)	χ^2 = 20.911	<0.001
Cortical irregularity without definite erosion, n (%)	13 (26.0)	8 (20.0)	10 (25.0)	χ^2 = 0.483	0.785

8.0%; P = 0.003), consistent with a more focal tendon-based lesion pattern. Acoustic behavior during real-time examination also differed significantly, with dynamic acoustic artifact enhancement observed more often in GA than in CT (84.0% vs. 70.0%; P = 0.002) (**Figure 2**).

Perilesional tissue reaction and secondary changes

Compared with CT, GA showed a lower frequency of perilesional edema (36.0% vs. 57.5%; P = 0.042) but a markedly higher frequency of synovial proliferation (48.0% vs. 7.5%; P< 0.001). In contrast, CT was characterized by more prominent tendon-related and peri-tendinous secondary changes, including tendon fiber disruption (19/40, 47.5% vs. 6/50, 12.0%; P<0.001), peritendinous fluid (16/40, 40.0% vs. 7/50, 14.0%; P = 0.005), adjacent bursitis (17/40, 42.5% vs. 8/50, 16.0%; P = 0.005), and dynamic pain elicited during probe compression (27/40, 67.5% vs. 14/50, 28.0%; P<0.001). By contrast, no significant between-group differences were observed for reactive hyperemia (12/40, 30.0% vs. 19/50, 38.0%; P = 0.169) or local provoked tenderness at the scan site (9/40, 22.5% vs. 16/50, 32.0%; P = 0.317) (**Figure 3**).

Composite imaging signatures differentiating GA and CT

GA was characterized predominantly by crystal deposition along synovial and cartilage-related structures, including a markedly higher prevalence of the double-contour sign (58.0% vs. 2.5%, P<0.001), synovial-based deposits (70.0% vs. 5.0%, P<0.001), heterogeneous aggregate patterns (68.0% vs. 25.0%, P<

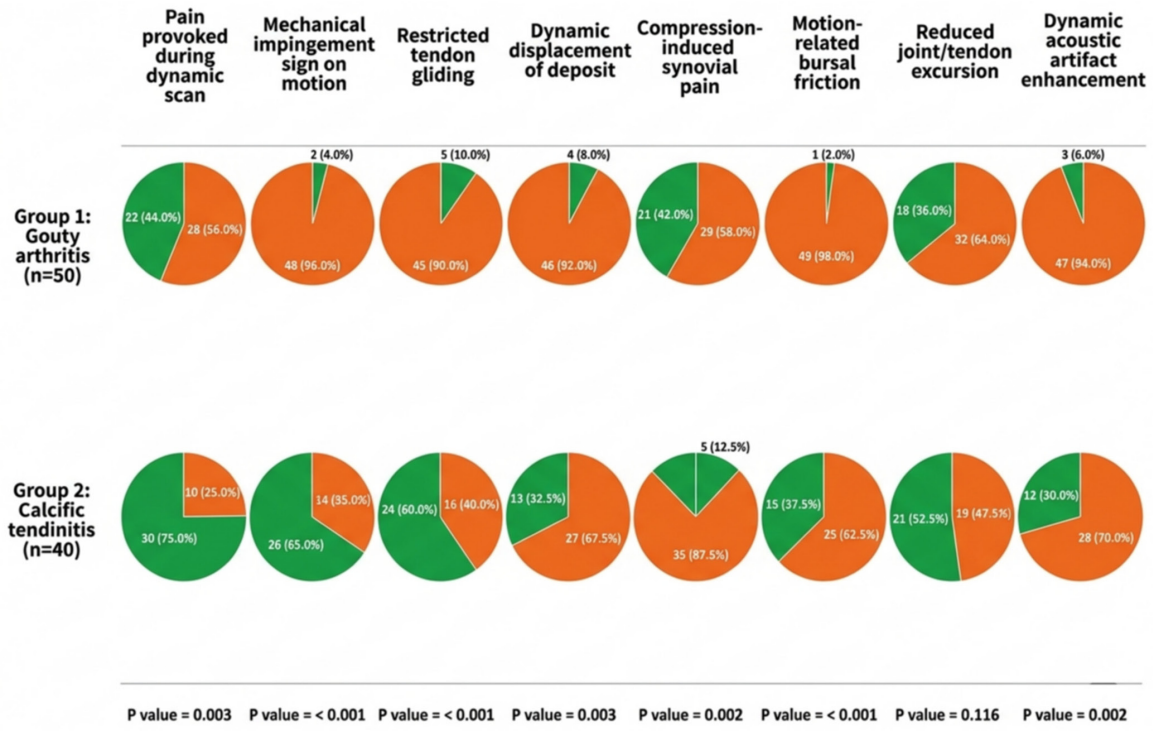

Figure 2. Dynamic ultrasound findings.

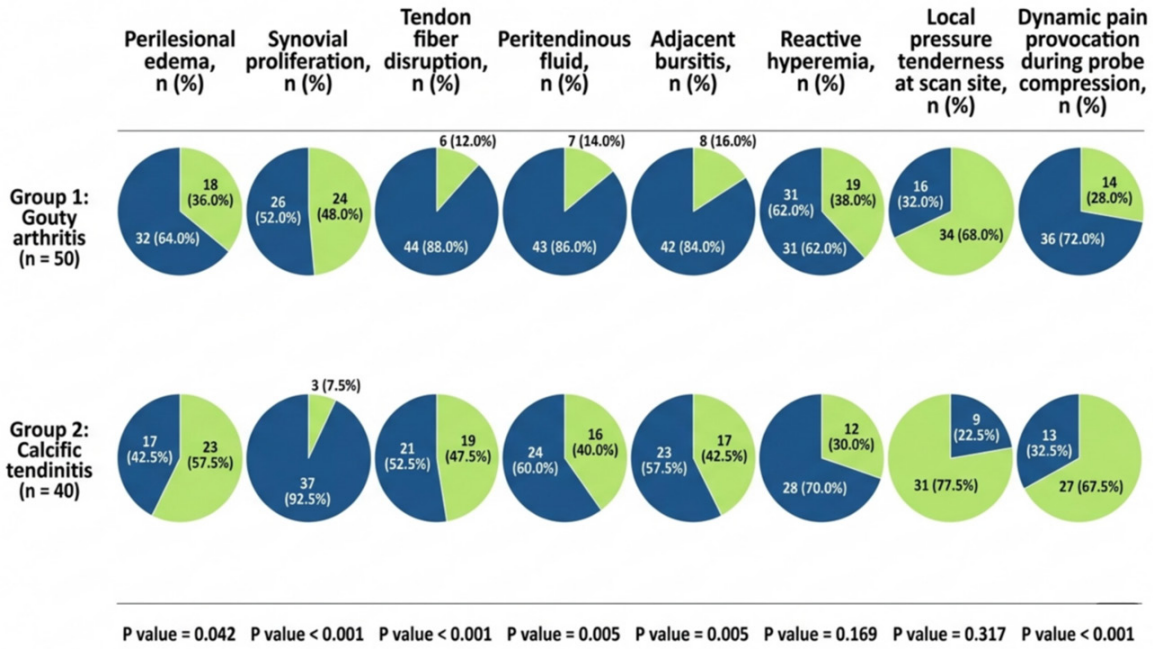

Figure 3. Perilesional tissue reaction and secondary changes.

0.001), multifocal distribution (58.0% vs. 27.5%, P = 0.004), bone erosion (30.0% vs. 5.0%, P = 0.003), and cartilage surface deposition (52.0% vs. 2.5%, P<0.001). By contrast, CT exhibited a distinct calcific phenotype dominated by intratendinous involvement, with

Table 5. Composite imaging signatures differentiating gouty arthritis and calcific tendinitis

Imaging signature component	Group 1: Gouty arthritis (n = 50)	Group 2: Calcific tendinitis (n = 40)	χ^2	*P* value
Double-contour sign present, n (%)	29 (58.0)	1 (2.5)	30.803	<0.001
Synovial-based deposit, n (%)	35 (70.0)	2 (5.0)	38.781	<0.001
Intratendinous embedded deposit, n (%)	9 (18.0)	35 (87.5)	42.957	<0.001
Arc-shaped calcification, n (%)	4 (8.0)	28 (70.0)	37.280	<0.001
Posterior acoustic shadowing, n (%)	10 (20.0)	31 (77.5)	29.623	<0.001
Heterogeneous aggregate pattern, n (%)	34 (68.0)	10 (25.0)	16.444	<0.001
Bone erosion, n (%)	15 (30.0)	2 (5.0)	9.065	0.003
Multifocal distribution, n (%)	29 (58.0)	11 (27.5)	8.372	0.004
Shoulder-dominant involvement, n (%)	3 (6.0)	37 (92.5)	67.340	<0.001
Cartilage surface deposition, n (%)	26 (52.0)	1 (2.5)	25.929	<0.001

substantially higher frequencies of intratendinous embedded deposits (87.5% vs. 18.0%, P<0.001), arc-shaped calcification (70.0% vs. 8.0%, P<0.001), posterior acoustic shadowing (77.5% vs. 20.0%, P<0.001), and shoulder-dominant involvement (92.5% vs. 6.0%, P< 0.001) (**Table 5**).

ROC analysis

Among all evaluated features, shoulder-dominant involvement showed the highest diagnostic accuracy, with an AUC of 0.932 (95% CI, 0.880-0.984; P<0.001), indicating excellent discrimination. This was followed by intratendinous deposit (AUC = 0.848, 95% CI, 0.768-0.927; P<0.001) and synovial involvement (AUC = 0.825, 95% CI, 0.738-0.911; P<0.001), both of which also demonstrated strong diagnostic utility. Arc-shaped calcification yielded good performance (AUC = 0.810, 95% CI, 0.721-0.899; P<0.001), whereas posterior acoustic shadowing (AUC = 0.788, 95% CI, 0.692-0.884; P<0.001) and the double-contour sign (AUC = 0.778, 95% CI, 0.679-0.877; P<0.001) provided moderate discriminatory value. Similarly, cartilage surface deposition (AUC = 0.748, 95% CI, 0.646-0.850; P<0.001) and heterogeneous aggregate pattern (AUC = 0.715, 95% CI, 0.608-0.822; P<0.001) remained significantly informative, although with comparatively lower accuracy (**Figure 4**). Overall, the ROC analysis indicates that topographic distribution, particularly shoulder predominance, together with lesion localization and morphologic calcific patterns, offers the most robust diagnostic framework for differentiating CT from GA on HFUS.

Multivariable logistic regression for differentiating GA from CT

In the adjusted model, the double-contour sign (adjusted OR, 7.861; 95% CI, 2.752-22.460; P<0.001), synovial involvement (adjusted OR, 0.908; 95% CI, 0.852-0.968; P = 0.003), cartilage surface deposition (adjusted OR, 0.206; 95% CI, 0.080-0.529; P = 0.001), intratendinous deposit (adjusted OR, 3.277; 95% CI, 1.233-8.713; P = 0.017), posterior acoustic shadowing (adjusted OR, 1.431; 95% CI, 1.222-1.676; P<0.001), and shoulder-dominant involvement (adjusted OR, 2.677; 95% CI, 1.819-3.941; P<0.001) remained independently associated with the final model (**Table 6**).

Representative HFUS images of crystal deposition in the knee joint

Representative HFUS images of the knee joint further illustrated the distinct deposition patterns observed in GA and CT. In GA, the lesion appeared as linear and irregular hyperechoic deposition distributed along the synovial/cartilage surface, consistent with the typical surface-oriented pattern of monosodium urate crystal accumulation (**Figure 5A**). By contrast, CT showed a more localized and compact hyperechoic lesion within the tendon, with clear caliper-based measurement, supporting a focal intratendinous calcific deposition pattern. These representative images visually reflect the different crystal-tissue interfaces in the two diseases, with GA characterized by articular or synovial surface involvement and CT characterized by discrete tendon-based calcification (**Figure 5B**).

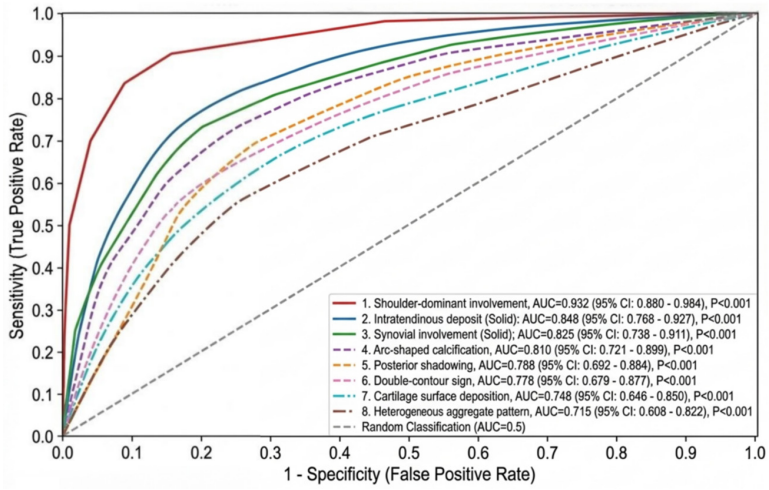

Figure 4. ROC curve.

Discussion

This study indicates that HFUS can discriminate between GA and CT using a reproducible set of topographic, morphologic, quantitative, and dynamic imaging features, rather than an isolated single sonographic appearance. The main novelty of the current work is to go beyond the description of individual diseases in favor of a comparative diagnostic pattern: GA presented synovial- and cartilage-based, multifocal, smaller yet more irregular deposits with more intense intra-articular inflammatory activity in the background, whereas CT presented a tendon-based, shoulder-predominant, larger and more echogenic calcific pattern with pronounced posterior acoustic shadowing and secondary peri-tendinous alterations. Notably, these observations were narrowed down to a clinically actionable set of signature features, with the double-contour sign, synovial involvement, and cartilage surface deposition identified as independent predictors of GA, and intratendinous deposit, posterior acoustic shadowing, and shoulder-dominant involvement as independent predictors of CT, using ROC and multivariate analyses. Collectively, these results support the notion that HFUS can capture disease-specific crystal-tissue interactions and could be used as a noninvasive imaging modality in routine practice to differentiate these conditions.

One of the major conclusions of this study is the centrality of lesion distribution in discriminating GA and CT. Previously available ultrasound evidence has largely demonstrated that gout localizes predominantly to synovial-lined structures, hyaline cartilage surfaces, tendon sheaths, and lower-extremity joints, whereas CT is most commonly seen in the rotator cuff tendons and surrounding bursae [15, 16]. Our findings clearly fit into that framework but go a step further by demonstrating that the topography of the two diseases is a highly diagnostic item, with shoulder-dominant involvement having the largest AUC and being independently associated with CT after adjustment. The mechanisms presumably reflect the distinct tissue niches of monosodium urate and hydroxyapatite crystal deposition: urate supersaturation and microenvironmental conditions in gout support periarticular and cartilaginous deposition, whereas hydroxyapatite deposition in CT favors tendon degeneration, fibrocartilaginous conversion, hypoxia, and unsuccessful remodeling, particularly in the supraspinatus region [17]. The clinical implication is obvious: ultrasound interpretation must start with “Where is the crystal?” and then “What does the crystal look like?”, since the anatomical setting significantly changes the diagnostic likelihood compared with over-reliance on a single sign.

The two conditions differ in the morphology and quantitative architecture of deposits. Gout deposits have been previously reported as tophaceous, clustered, or superficially layered, whereas CT deposits are compact, well-defined, and highly reflective [18]. This difference is further supported by our data, which indicated that CT deposits were larger, deeper, more uniform, and more echogenic, whereas GA lesions were more numerous, superficial, fragmented, and disordered, with wider surface coverage along cartilage or tendon interfaces. These differences likely arise from variations in crystal composition and growth patterns. Hydroxyapatite tends to deposit as highly mineralized intratendinous foci, which can create high acoustic impedance disparities and posterior shadowing, whereas monosodium urate is more apt to form microaggregates, surface

Table 6. Multivariable logistic regression for differentiating gouty arthritis from calcific tendinitis

Predictor	Adjusted OR	95% CI	*P* value
Double-contour sign	7.861	2.752-22.460	<0.001
Synovial involvement	0.908	0.852-0.968	0.003
Cartilage surface deposition	0.206	0.080-0.529	0.001
Intratendinous deposit	3.277	1.233-8.713	0.017
Posterior acoustic shadowing	1.431	1.222-1.676	<0.001
Shoulder-dominant involvement	2.677	1.819-3.911	<0.001

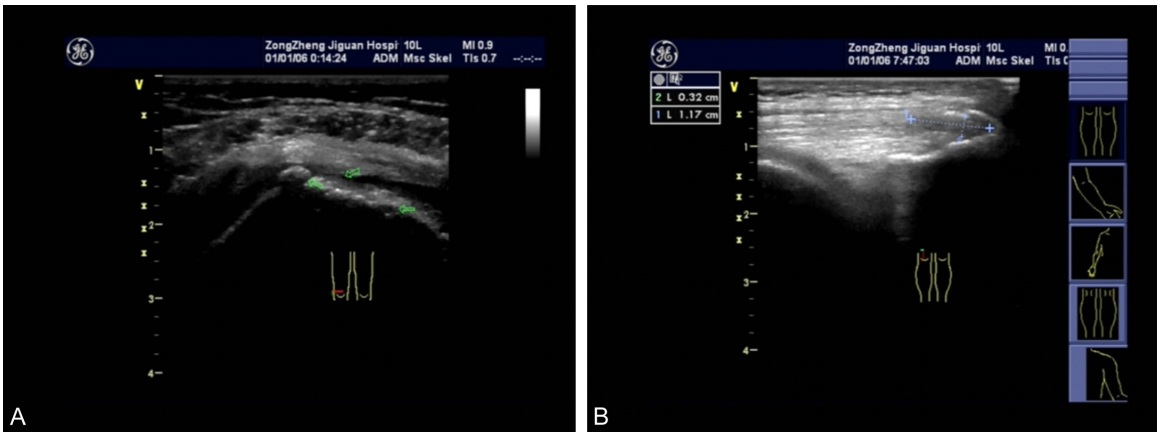

Figure 5. Representative high-frequency ultrasound images of crystal deposition in the knee joint. A. Gouty arthritis, demonstrating hyperechoic deposits distributed along the synovial/articular surface (arrows). B. Calcific tendinitis, demonstrating a localized intratendinous hyperechoic calcific lesion with imaging measurement.

layer deposition, or periarticular infiltration that spreads along biologic interfaces rather than as a single dense calcific mass. This difference has significant interpretive implications: a smaller lesion should not be considered clinically less informative, as the pattern of irregularity, multiplicity, and surface extension can be more diagnostically informative than lesion size alone in GA.

The associated inflammatory environment provides another set of discriminatory data on top of crystal visualization. Earlier research on gout ultrasound has focused on synovial hypertrophy, effusion, Doppler activity, and erosion [19, 20], whereas the literature on CT has highlighted features like peri-tendinous edema, bursitis, tendon thickening, and pain associated with the resorptive component of the calcification process [21]. The current findings substantiate both paradigms and make it clear that they can be directly used in the differential diagnosis: GA exhibited an intra-articular inflammatory phenotype, whereas CT presented a peri-tendinous and bursal reaction pattern. This is biologically reasonable, as monosodium urate crystals are potent stimulators of inflammasome-mediated synovitis and repetitive intra-articular inflammatory responses, whereas hydroxyapatite deposition leads to a localized tendon-bursal reaction, particularly when the calcific contents extrude or enter an inflammatory resorption phase. Clinically, these results caution against treating inflammatory changes generically; the compartment in which inflammation is detected, whether synovial or peritendinous, may be as informative as the degree of inflammation itself.

The dynamic ultrasound results represent an additional element of novelty and one of the more valuable clinical implications of this work. Most of the literature on crystal arthropathy imaging involves static structural observation, but dynamic analysis offers the opportunity to observe mechanical behavior reflecting lesion anchorage, tissue interaction, and symptom provocation. GA more often revealed pain provocation, restricted gliding, mechanical impingement, compression-induced synovial pain, and

motion-specific bursal friction, whereas CT more often revealed dynamic displacement of the deposit. The most likely explanation is that GA-related deposition is embedded in an inflamed synovial or articular soft-tissue milieu that restricts motion and enhances pain through inflammatory sensitization, whereas CT lesions behave as more focal intratendinous calcific bodies, the motion or compression of which produces local mechanical symptoms. These observations indicate that dynamic HFUS should not be regarded as an optional application; it can enhance diagnostic sensitivity in uncertain cases and provide a means to separate morphology from symptom generation in real time.

The results of the diagnostic modeling have direct translational impact, as they define an imaging framework that can be applied at the point of care. Current diagnostic pathways for GA and CT often rely on aspiration, radiography, dual-energy CT, or serial clinical follow-up, each of which has feasibility drawbacks related to invasiveness, cost, availability, or inability to characterize soft tissues dynamically. Our study supports a more organized sonographic decision strategy by demonstrating that a limited number of HFUS characteristics can independently classify disease phenotype. Mechanistically, this is a powerful approach because the retained predictors map onto the biologic niche of each crystal type: cartilage and synovium for urate, tendon and dense calcification for hydroxyapatite. The broader implication is that HFUS can reduce time to diagnosis, enhance targeting of aspiration or complementary imaging, and decrease inappropriate urate-lowering therapy when clinical manifestations are atypical. Meanwhile, the results caution sonographers and clinicians to remain vigilant about disease context, as high-performing features in one group may not perform as well in patients with mixed crystal disease, advanced degeneration, or other atypical anatomical presentations.

Several limitations of this work should be acknowledged. First, this was a single-center retrospective study with a relatively small sample, which may limit external validity and could lead to model instability, as reflected by wide confidence intervals for some multivariate estimates. Second, not every diagnosis was substantiated by crystal analysis, which may have introduced incorporation bias in cases diagnosed by clinicoradiologic criteria alone. Third, typical disease phenotypes such as shoulder-predominant CT and lower-extremity-predominant GA were preferentially included, which may overestimate diagnostic separation compared with more heterogeneous real-world cohorts. Fourth, ultrasound is operator-dependent, and the current analysis did not fully address interobserver reproducibility of the proposed imaging signatures or quantitative metrics. Fifth, because this was a cross-sectional study, we were unable to assess changes in deposit morphology across disease stages, treatment response, or recurring flare/resorptive episodes. Future multicenter prospective research involving standardized image acquisition, blinded reading, external validation, and, where possible, crystal confirmation is needed to validate the robustness and generalizability of this HFUS diagnostic framework.

In conclusion, this research indicates that GA and CT have distinct and biologically consistent HFUS phenotypes that can be used to achieve differential diagnosis. GA is characterized by multifocal deposition involving synovial membranes and cartilage with irregular superficial spreading, whereas CT is characterized by shoulder-dominant intratendinous calcification with larger, denser, more echogenic deposits and pronounced posterior acoustic shadowing. The combination of lesion location, deposit morphology, inflammatory context, and dynamic behavior offers a stronger diagnostic framework than any single sign alone. These results support the use of HFUS as an effective, noninvasive, and clinically informative imaging modality to differentiate between two common crystal deposition disorders and provide a basis for more standardized imaging-based diagnostic algorithms.

Disclosure of conflict of interest

None.

Address correspondences to: Wei Wang, Department of Medical Technology Support, Jingzhong Medical Area, PLA General Hospital, No. 21 Andingli North Street, Dongcheng District, Beijing 100120, China; Tel: +86-010-66795740; E-mail: wwbj2026@163.com; Hongyan Zhao, Department

of Lishilu Outpatient, Jingzhong Medical Area, PLA General Hospital, No. 23 Headlines, Nanlishi Road, Xicheng District, Beijing 100842, China. Tel: +86-13581625755; E-mail: 1315154388@qq.com; Hehuan Zhang, Department of Zhantansi Outpatient, Jingzhong Medical Area, PLA General Hospital, 3rd Floor, No. 2 Aimin Street, Xicheng District, Beijing 100034, China. Tel: +86-18210827330; E-mail: 564978605@qq.com

References

[1] Galozzi P, Bindoli S, Luisetto R, Sfriso P, Ramonda R, Scanu A and Oliviero F. Regulation of crystal induced inflammation: current understandings and clinical implications. Expert Rev Clin Immunol 2021; 17: 773-787.

[2] Towiwat P, Chhana A and Dalbeth N. The anatomical pathology of gout: a systematic literature review. BMC Musculoskelet Disord 2019; 20: 140.

[3] Darrieutort-Laffite C, Blanchard F and Le Goff B. Calcific tendonitis of the rotator cuff: from formation to resorption. Joint Bone Spine 2018; 85: 687-692.

[4] Bove M, Cicero AF, Veronesi M and Borghi C. An evidence-based review on urate-lowering treatments: implications for optimal treatment of chronic hyperuricemia. Vasc Health Risk Manag 2017; 13: 23-28.

[5] Dehlin M, Jacobsson L and Roddy E. Global epidemiology of gout: prevalence, incidence, treatment patterns and risk factors. Nat Rev Rheumatol 2020; 16: 380-390.

[6] Bazzocchi A, Pelotti P, Serraino S, Battaglia M, Bettelli G, Fusaro I, Guglielmi G, Rotini R and Albisinni U. Ultrasound imaging-guided percutaneous treatment of rotator cuff calcific tendinitis: success in short-term outcome. Br J Radiol 2016; 89: 20150407.

[7] Saran S, Babhulkar JA, Gupta H and Chari B. Imaging of calcific tendinopathy: natural history, migration patterns, pitfalls, and management: a review. Br J Radiol 2024; 97: 1099-1111.

[8] Butt A, Umaskanth N and Sahu A. Image-guided intervention in the management of chronic patellar tendinopathy with calcification: a three-pronged approach. BMJ Case Rep 2021; 14: e240553.

[9] Vassalou EE, Klontzas ME, Plagou AP and Karantanas AH. Ultrasound-guided percutaneous irrigation of calcific tendinopathy: redefining predictors of treatment outcome. Eur Radiol 2021; 31: 2634-2643.

[10] Albano D, Aringhieri G, Messina C, De Flaviis L and Sconfienza LM. High-frequency and ultra-high frequency ultrasound: musculoskeletal imaging up to 70 MHz. Semin Musculoskelet Radiol 2020; 24: 125-134.

[11] Izzetti R, Vitali S, Aringhieri G, Nisi M, Oranges T, Dini V, Ferro F, Baldini C, Romanelli M, Caramella D and Gabriele M. Ultra-high frequency ultrasound, a promising diagnostic technique: review of the literature and single-center experience. Can Assoc Radiol J 2021; 72: 418-431.

[12] Lee YH and Song GG. Diagnostic accuracy of ultrasound in patients with gout: a meta-analysis. Semin Arthritis Rheum 2018; 47: 703-709.

[13] Catapano M, Robinson DM, Schowalter S and McInnis KC. Clinical evaluation and management of calcific tendinopathy: an evidence-based review. J Osteopath Med 2022; 122: 141-151.

[14] Hegazi T. Hydroxyapatite deposition disease: a comprehensive review of pathogenesis, radiological findings, and treatment strategies. Diagnostics (Basel) 2023; 13: 2678.

[15] Yuan Y, Liu C, Xiang X, Yuan TL, Qiu L, Liu Y, Luo YB, Zhao Y and Herrmann M. Ultrasound scans and dual energy CT identify tendons as preferred anatomical location of MSU crystal depositions in gouty joints. Rheumatol Int 2018; 38: 801-811.

[16] Catapano M, Robinson DM, Schowalter S and McInnis KC. Clinical evaluation and management of calcific tendinopathy: an evidence-based review. J Osteopath Med 2022; 122: 141-151.

[17] Sudoł-Szopińska I, Lanckoroński M, Teh J, Diekhoff T, Giraudo C and Chaudhary SR. Advanced imaging of gout and other inflammatory diseases around the knee. Semin Musculoskelet Radiol 2024; 28: 337-351.

[18] Parathithasan N, Lee WK, Pianta M, Oon S and Perera W. Gouty arthropathy: review of clinicopathologic and imaging features. J Med Imaging Radiat Oncol 2016; 60: 9-20.

[19] Pârvănescu CD, Bărbulescu AL, Biță CE, Dinescu ȘC, Trașcă BA, Firulescu SC and Vreju FA. Ultrasound features in gout: an overview. Med Sci (Basel) 2024; 12: 37.

[20] Yang L, Wang Z, Yao Z and Cui LG. The evolving role of musculoskeletal ultrasound in gout: from diagnosis to management-a narrative review. J Ultrasound Med 2026; 45: 1351-1363.

[21] Koneru BN, Barron DA, Muecke R, Shaffer R, Thomas TO, Sonnhoff M, Blach RM, Steike DR, Deloch L, Singh PK and Seegenschmiedt H. Periarticular soft tissue disorders: enthesopathies, tendinopathies, and bursitis-pathophysiology and radiotherapeutic approaches. Semin Radiat Oncol 2026; 36: 48-60.